Volume 14 | Number 24 | 28 June 2018 | Pages 4883–5152

Soft Matter

rsc.li/soft-matter-journal

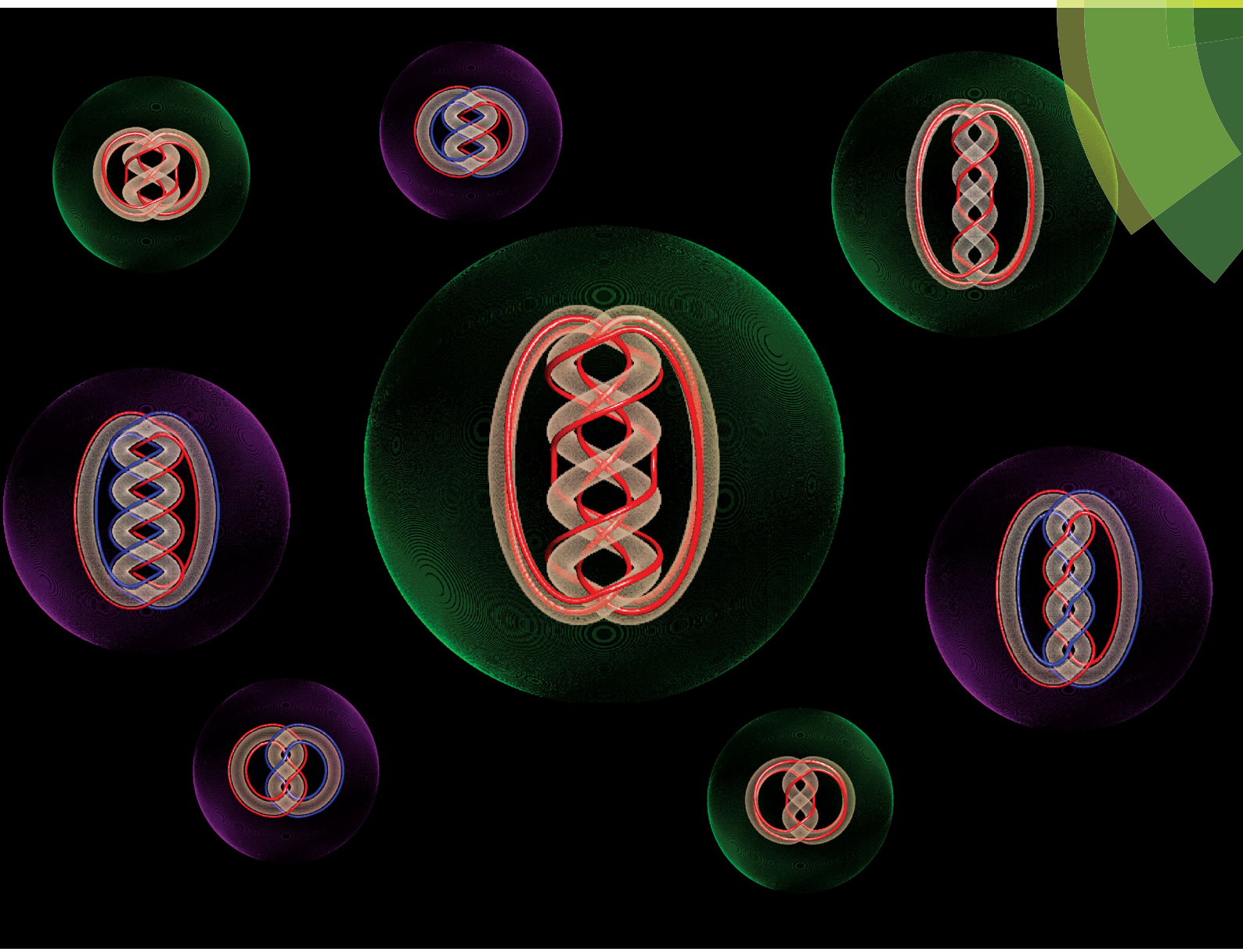

ISSN 1744-6848

ROYAL SOCIETY OF CHEMISTRY

PAPER
S. Masoomeh Hashemi and Miha Ravnik
Nematic colloidal knots in topological environments

Soft Matter

PAPER

View Article Online
View Journal | View Issue

Cite this: *Soft Matter*, 2018, **14**, 4935

Nematic colloidal knots in topological environments

S. Masoomeh Hashemi *[a] and Miha Ravnik [bc]

The role of environment in shaping material properties is of great significance, but less is known about how non-trivial topology of the environment couples to material states, which can be of non-trivial topology themselves. In this paper, we demonstrate the role of the topology of the environment on the formation of complex nematic fields and defect structures, specifically in the system of nematic colloidal knots. The topological environments around knotted colloidal particles are suggested to exist as spherical surface-patterned nematic cavities imposing radial, uniform or hyperbolic nematic profiles. We show that topologically different nematic environments significantly affect and create differences in the colloidal field structure created within the environment, such as the location, profile and number of topological defects. Specifically, we demonstrate that topological environments in combination with knotted colloidal particles of non-trivial topology lead to the formation of diverse nematic knotted and linked fields. These fields are different adaptations of the knotted shape of the colloidal particles, creating knots and links of topological defects as well as escaped-core defect-like solitonic structures. These are observed in chiral nematic media but here are stabilised in achiral nematic media as a result of the distinct shape of the knotted colloidal particle, with a double helix segment and nematic environmental patterns. More generally, this paper is a contribution towards understanding the role of environment, especially its topology, on the response and defect formation in elastic fields, such as in nematic liquid crystal colloids.

Received 16th March 2018,
Accepted 21st April 2018

DOI: 10.1039/c8sm00539g

rsc.li/soft-matter-journal

1 Introduction

An inseparable element in the design of topological soft materials is the environment – for example, imposed by the surface, confinement or geometry – which on one hand can pose constraints on the material design but on the other hand can generate possibilities for new material structures.[1–3] A common role of the environment in the design of topological soft matter is that it primarily affects the energetics of the material, such as making structures stable or metastable. However, less is known about the role of the topology of the environment on material design. For example, it has been shown that topological design of lattices, environments and boundaries can increase the stability and optimize the proficiency of materials or even create materials with novel properties, for example in topological insulators,[4,5] topological superconductors and superfluids[6] and liquid crystal colloids.[7–10]

The topology of the material or material system – such as knottedness or entanglement – can profoundly influence both the static and dynamic properties of the system.[11,12] Examples of knotted molecular systems include knots of DNA rings,[13] knots of cyclic RNA molecules,[14] polymer knots[15] and template-synthesized molecular knots.[16] While tying threads in a filamentous material is a local task, further fascinating realizations of knots and links have also emerged in knotted fields where the entire field space of the system is effectively tied into a knot or link. Knotted fields are observed in vortex-shaped textures in optics,[17] superfluids,[18] superconductors,[19] velocity fields in fluid dynamics,[20] and knotted solitons and knotted topological defect lines in nematic liquid crystals.[9,10,21–25] It has been shown that the classification of such topological systems is given by topological conservation laws and depends on topological invariants, such as knot polynomials and the crossing number of the knots.[26,27]

Complex nematic fluids are shown to stabilise a variety of topological structures spanning from solitonic structures like skyrmions, merons, torons and hopfions[28–35] to different forms of defect points and lines.[36–38] These topological structures can form either spontaneously or by localized inclusions, such as with colloidal particles.[9,10,22] Knots and links with diverse morphologies have been realised in chiral and achiral nematic systems using different colloidal and confining surfaces and under different surface ordering fields, which is known as

[a] *Faculty of Mathematics and Physics, University of Ljubljana, Jadranska 19, Ljubljana, 1000, Slovenia. E-mail: hashemy.m@gmail.com*
[b] *Faculty of Mathematics and Physics, University of Ljubljana, Jadranska 19, Ljubljana 1000, Slovenia*
[c] *Jozef Stefan Institute, Jamova 39, Ljubljana 1000, Slovenia*

surface anchoring. An example is the induction of knot solitons by localized vortex laser beams in a chiral nematic medium that is confined in a uniform cell.[21] In addition, there are several examples of knotted and linked defect lines, such as those formed around soft lattices of spherical colloidal particles that are confined in a twisted nematic cell,[9] imprinted by knotted, linked and non-orientable colloidal particles,[10,22,39] generated by temperature quenching in handlebody nematic droplets with a normal anchoring condition[23] or formed in a spherical chiral nematic droplet with normal anchoring and surrounded by solitonic structures as scaffolds.[24,25] More generally, these studies show that topological soft materials can be used and perform as an exciting and advanced topological platform.

A variety of methods and approaches have been developed for the control of the environment of soft materials, such as the properties of the dispersion, bounding surfaces, and the role of external or internal fields.[40,41] Nematic system approaches for controlling or designing the environment include photo-polymerization, nanolithography, microfluidic synthesis, emulsification, microscopy, surface anchoring techniques and theoretical modelling methods.[7,9,10,21,31,42,43] Besides extensive studies on the different shapes of colloidal and confining surfaces, recent achievements have allowed for the controlled production of polymer- and other liquid-dispersed nematic droplets with different shapes, anchoring patterns and consequently different total topological charges.[43–46] Naturally, such droplets serve as controllable environments as, for example, their structure may be used to control chemical reactions.[43] The production of spherical nematic droplets with surfactant-induced, pure, planar, degenerate and homeotropic anchorings is well established.[47,48] However, the production of well-defined patchy droplets is more challenging because of the deformability and fluidity of liquid surfaces. Two methods have been developed for controlling surface anchoring into a composite anchoring pattern. The first method employs ionic surfactants to make the droplets' anchoring pattern modifiable under the application of a dc electric field.[45] The second method is a mechanical modification technique in which the anchoring pattern is dynamically modified through the diffusion of droplets from a layer of sodium dodecyl sulfate (SDS), where they have a homeotropic anchoring, into a layer of pure glycerol, inducing planar degenerate anchoring.[43] Hence, patchy droplets with well-defined fractions of homeotropic and degenerate planar anchoring can be generated at the interface between SDS and glycerol, and upon photo-polymerization the patches can be created with a desired relative size. More generally, these recent developments clearly show that anchoring patterns can be controllably designed at a complex level.

In this paper, we explore the role of the topology of the environment on the formation and stabilisation of complex nematic fields and defect structures, specifically in the system of nematic colloidal knots confined within a spherical cavity of non-trivial surface-imposed topology fields. Using mesoscopic finite difference numerical modelling based on the phenomenological Landau-de Gennes theory, different types of knots, links and other nematic topological structures are observed, which are affected by different environment-imposed topological charges and are tailored by trefoil and pentafoil knotted colloidal particles with a double helix segment. Specifically, we observe a richness of simple (a few crossings) to complex (a few tens of crossings) knotted and linked $-1/2$-defect loops with partial/piecewise twisted cores, in addition to escaped-core twisted solitonic structures. We show that different, although smoothly-varying, environmental nematic patterns can cause significant differences in the structure, location and number of the topological defects. We also show that, in the case of the specific shape of the knotted colloidal particles with a double helix segment, by changing the geometric parameters of the double helix while keeping the topology of the system the same, different topological structures/states can be imprinted in the nematic environments. We illustrate that these differences between the topological states originate from an interplay between the screening ability of the particle and the nematic ordering effects of the environment.

2 Model and methods

The interconnection between the topological structure of a nematic environment and imprinted defect knots and links is explored by introducing trefoil and pentafoil knotted particles, which are made of double helix segments, into three different topological environments. To model the topological environments, we choose a spherical nematic cavity for confinement with three different anchoring patch patterns that effectively impose uniform, radial and hyperbolic bulk fields of 0, +1 and -1 net topological charge, respectively. The particles are taken as rigid and their surfaces are assumed to impose strong homeotropic anchoring.

The nematic field configurations are calculated by finite difference numerical minimization of the Landau-de Gennes phenomenological free energy[49] using an explicit method on a cubic mesh.[50] The free energy of the nematic within the single elastic constant approximation is given as

$$F = \int_{\text{bulk}} \mathrm{d}V \left(\frac{A}{2} Q_{ij} Q_{ji} + \frac{B}{3} Q_{ij} Q_{jk} Q_{ki} + \frac{C}{4} \left(Q_{ij} Q_{ji} \right)^2 + \frac{L}{2} \frac{\partial Q_{ij}}{\partial x_k} \frac{\partial Q_{ij}}{\partial x_k} \right). \quad (1)$$

where Q_{ij} is the order parameter tensor, with the eigenvector corresponding to the largest eigenvalue (mainly given by the nematic degree of order S) giving the average molecular orientation called the director $\boldsymbol{n}$. We use the following material constants $A = -0.172 \times 10^6$ J m^{-3}, $B = -2.12 \times 10^6$ J m^{-3}, $C = 1.73 \times 10^6$ J m^{-3} and $L = 4 \times 10^{-11}$ N which correspond to a standard thermotropic nematic material.[50] Strong anchoring on all surfaces including the environment sphere is assumed. Relaxing the system from different initial conditions is used to generate different configurations, effectively using the relaxation dynamics of the nematic field (*i.e.* nematic rotational dynamics without flow) for directing the system toward different possible topological states (further details given in ref. 50). We adapted Gmsh[51] shape and geometry generation and visualization software to work with the finite difference method. To visualize the

chiral features in the nematic textures, a scalar twist parameter is used, which is defined as $S_{TW} = \varepsilon_{ikl}Q_{ij}\partial Q_{lj}/\partial x_k$ as shown in ref. 52.

The knotted particles considered here are characterized using several geometric parameters including the thickness of the particle's tube and the radius, pitch and number of turns of its double helix segment. We selected a tube diameter of $2R/\xi = 12$, and we observed no significant changes in the topological states of the cavities by increasing or decreasing the thickness of the colloidal tubes on the tube diameter of $2R/\xi = 12$. We avoid the limits of highly compressed or highly stretched double helices and choose a ratio between the pitch and the diameter of the double helix of between two and three (the helical pitch $P/\xi = 60$), where the nematic field within the coils of the double helix are affected by both the particle and the environment. Therefore, from the four mentioned particle parameters, we only investigate the effect of the double helix diameter and the number of turns on the nematic textures. We investigate the double helix diameter $2R_{dh}/\xi = 36$ and $2R_{dh}/\xi = 21$ and we consider trefoil knots that have one helical turn or pentafoil knots that have two helical turns.

3 Spherical cavities with surface patches as topological environments

To create different topological environments we create spherical cavities that have surfaces dressed with uniform, radial or hyperbolic anchoring patterns characterized by the director variation $\boldsymbol{n_0} = (\sin\alpha\cos\beta,\ \sin\alpha\sin\beta,\ \cos\alpha)$ (Fig. 1a–c), where α and β are given in the spherical coordinates θ and ϕ as $\beta = s\phi + \beta_0$ and $\tan(\alpha/2) = (\tan(\theta/2))^{|s|}$, and s is the topological charge of the defect.[37] For instance, when $s = \pm 1$ and 0 (and taking $\beta_0 = 0$), this gives in Cartesian coordinates: uniform $\boldsymbol{n_0} = (0, 0, 1)$, radial $\boldsymbol{n_0} = (x/r, y/r, z/r)$, and hyperbolic $\boldsymbol{n_0} = (x/r, y/r, -z/r)$ patterns, where $r = (x^2 + y^2 + z^2)^{1/2}$. More formally, the total topological charge of the patterns within the cavity can be determined by taking the integral, $q_t = (1/4\pi)\int\int \mathrm{d}\theta\mathrm{d}\phi \boldsymbol{v}\left(\frac{\partial \boldsymbol{v}}{\partial\theta}\times\frac{\partial \boldsymbol{v}}{\partial\phi}\right)$, over a closed surface enclosing the pattern, where the sign of the topological charge is ambiguous due to the symmetry of the nematic director $\boldsymbol{n} \leftrightarrow -\boldsymbol{n}$.

Experimentally, such topology-imposing cavities for molecular-type nematics could possibly be generated using an approach presented in ref. 43. An exciting direction for imprinting a spatially varying surface anchoring profile was recently also shown using metasurfaces, where it was used with water-based chromonic liquid crystals.[53] For colloidal type nematics, patchy surface anchoring profiles could possibly also be created by controlling the surface morphology and roughness, which has been shown can lead to variable anchoring directions.[54–56]

Experimentally, topological environments could be created by generating patchy cavities with alternating planar and homeotropic anchorings (Fig. 1d), for example using an approach

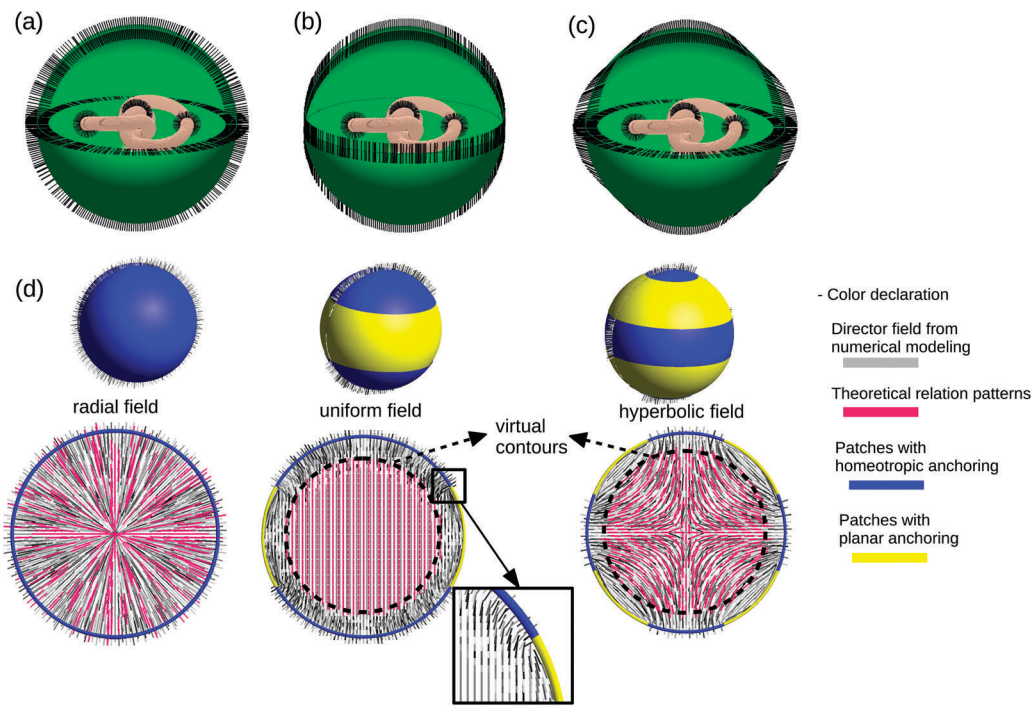

Fig. 1 Creation of topological environments through an anchoring design of the cavity surfaces. (a–c) Schematic view of the used spherical cavities (green surfaces) that impose radial, uniform or hyperbolic anchoring pattern (black short lines) filled with a knotted particle at the cavity center. (d) Effective generation of radial, uniform or hyperbolic environments in cavities with surface patches of alternating planar and homeotropic anchoring conditions. The patch arrangements used to create effective radial (well known, simple homeotropic anchoring all over the cavity surface), uniform (three patches) and hyperbolic (five patches) environments are shown in (d). Patches with homeotropic anchoring are shown in blue and patches with planar anchoring in yellow. Superimposed director fields from numerical modelling of the cavities with patchy surfaces (gray dashed lines) and theoretical radial, uniform and hyperbolic field configurations (pink dashed lines) show similar patterns inside the virtual contour.

presented in ref. 43. This approach is the production of patchy liquid crystal droplets inside alternating layers of different materials, such as pure glycerol and sodium dodecyl sulfate (SDS), that respectively impose planar and homeotropic anchorings on the surface of the droplet. To create radial, uniform and hyperbolic environments, cavities with all homeotropic anchoring, three patches and five patches with planar-homeotropic anchoring alternations can be used, as shown in Fig. 1d. Effectively, the surfaces of the patchy cavities impose no net topological charge in the case of a uniform profile, +1 charge in the radial profile, and −1 charge in the hyperbolic profile. To determine the regions with similar patterns to the radial, uniform and hyperbolic profiles, we illustrate the superimposed patterns from numerical modelling and theoretical relations on a diagonal cross section of the cavities (Fig. 1d). In the radial case, the profiles from numerical modelling and the theoretical pattern fully match all over the cavity, whereas in the uniform and hyperbolic cases, the numerical and theoretical patterns match inside a virtual spherical contour (Fig. 1d), so that the observed bulk nematic patterns within the patchy cavities are shown to be similar to the uniform and hyperbolic profiles.

4 Colloidal particles in topological environments

4.1 Spheres and tori

Rather simple shapes of colloidal particles – *i.e.* a sphere and a torus – are first put inside the radial, uniform and hyperbolic cavity, as shown in Fig. 2. The particles are assumed to have surfaces that impose strong homeotropic anchoring. In the case of the radial environment (Fig. 2a), the nematic profile is perfectly radial with no topological defect, as the particle effectively takes the role of a radial point defect that emerges in the center of an empty (*i.e.* without particles) cavity. The uniform environment (Fig. 2b) gives the well-known structure of a Saturn ring defect with the winding number −1/2, which encircles the spherical particle around its equator. For the hyperbolic environment (Fig. 2c), two defect rings are observed parallel to the equator at latitudes ±45° of the particle, both with the winding number −1/2, and are topologically equivalent to −1 bulk hyperbolic point defects. Toroidal colloidal particles with homeotropic anchoring are topologically neutral objects, *i.e.* they impose zero net topological charge *via* their

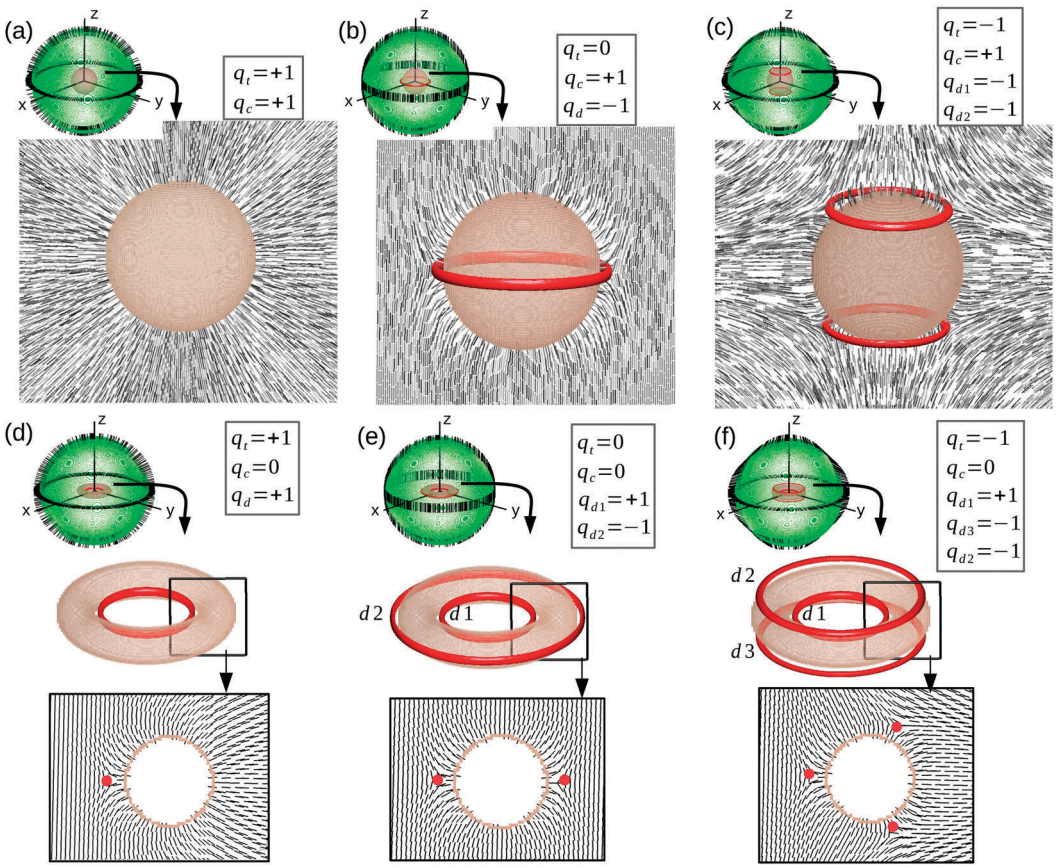

Fig. 2 Spherical and toroidal particles exposed to radial, uniform and hyperbolic environments. (a–c) Spherical particles and (d–f) toroidal particles inside radial, uniform and hyperbolic environments, accompanied with topological defect rings (regions with $S < 0.3$ that are shown in red) that compensate the cavity- and particle-imposed topological charges. Director fields (dashed lines in gray) are shown in a plane containing the rotational symmetry axis of the environments, and it can be seen that all defect rings have the winding number −1/2. The toroidal particles are shown in their stable states when the symmetry axis of the torus coincides with the symmetry axis of the environment. The topological charges regarding the environment q_t, the colloidal particle q_c and the defect rings q_d are also presented.

surface conditions. In Fig. 2d–f we present the nematic equilibrium states of toroidal particles in the radial, uniform and hyperbolic topological environments. Due to the different topology of the particle itself, the response of the nematic field is also different, and it essentially requires one more hyperbolic defect loop than the sphere in order to adapt to the radial, uniform or hyperbolic environment. To generalise, these simple cases with colloidal spheres and tori already show that the topological environment can directly affect the structure, location and number of topological defects in the nematic field.

In the present study, the colloidal particles are considered as rigid, while in a real system the colloidal particles exposed to a distorted nematic field could be deformable. The total elastic force exerted on a colloidal particle from a nematic environment can be calculated by integrating the Ericksen stress tensor σ_{ij} over the surface.[49,57] We calculate the local force per unit surface area on the surface elements of the particle, given by $d\mathcal{F}_i/dA = \sigma_{ij}\nu_j$, where ν_j denotes the normal to the surface. The local elastic forces per unit area acting at the particle surface in the radial, uniform and hyperbolic nematic environments are calculated to be of the order of magnitude of $5 \times 10^{-2}\frac{L}{\xi^2}$, where ξ is the nematic correlation length. In all three environments, the profile of the local forces on the colloidal surface is seen to be also nonhomogeneous, which may affect the shape of the particles, depending on the degree of the particle's deformability.

4.2 Trefoil and pentafoil knotted colloidal particles

The role of the topology of the environment on the complex nematic field and defect structures can be further demonstrated by considering colloidal particles in the shape of knots (for example, knotted particles were recently reported in ref. 10). We choose

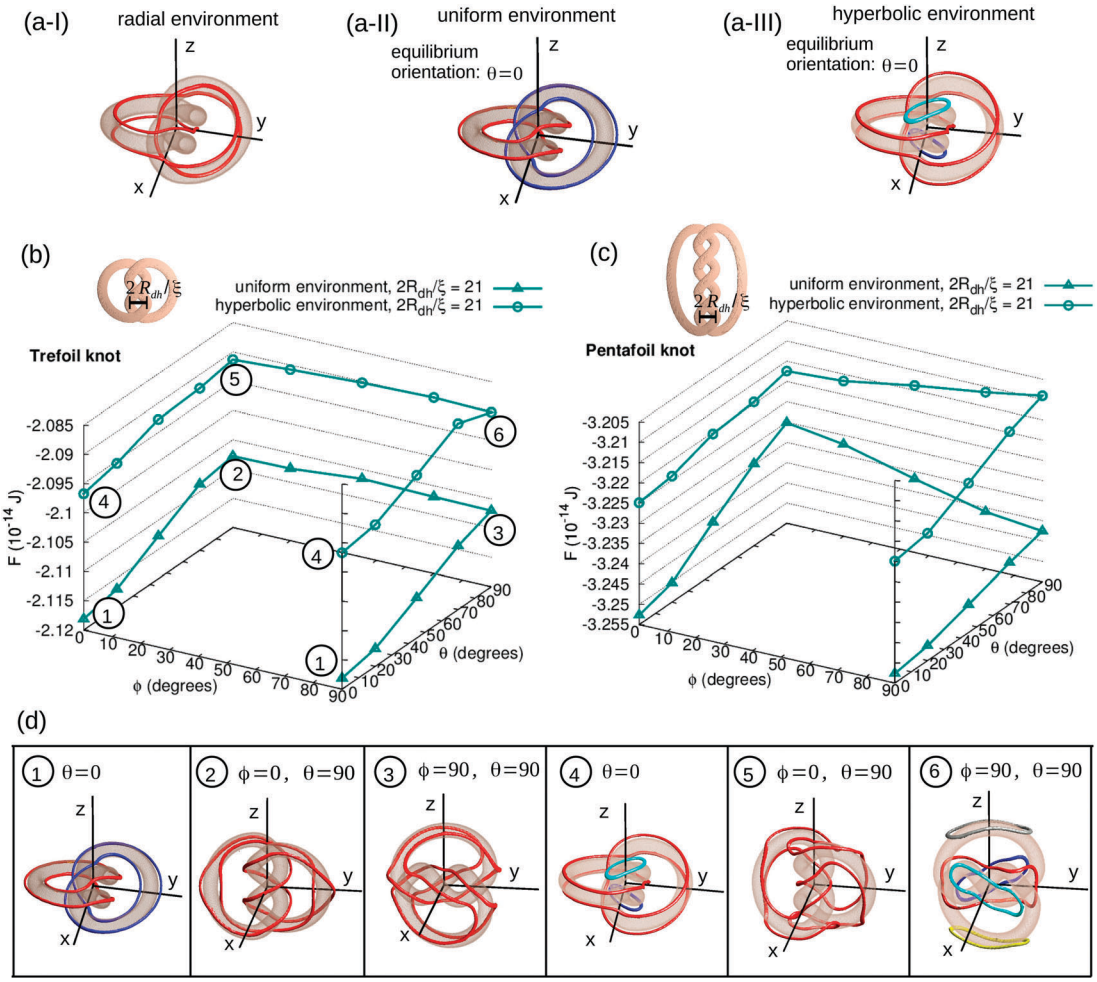

Fig. 3 Role of particle orientation on the topological states of the nematic knotted colloids in radial, uniform and hyperbolic environments. (a) The most stable state and the defect loops (isosurfaces with S = 0.3 in red, light blue and dark blue colors) related to the trefoil knotted particle with $2R_{dh}/\xi$ = 21 in radial, uniform and hyperbolic environments. (b and c) Free energy with respect to the orientation angle of the trefoil and pentafoil knotted particles, with $2R_{dh}/\xi$ = 21 when the particles are located at the cavity center in the uniform and hyperbolic environments. The graphs show that the energetically stable orientation of a knotted particle is always at θ = 0. As a typical example to show the orientation dependency of the topological states, the defect loops regarding four different orientations of a trefoil knotted particle in the uniform and hyperbolic environments from graph (b) are presented in (d). The defect loops are shown by the isosurface with S = 0.3 and are in red, light blue, dark blue, yellow and gray colors in order to indicate different closed loops.

individual colloidal particles in the shape of trefoil and pentafoil knotted colloidal particles with homeotropic anchoring conditions. Each of these knotted colloidal particles consists of a circular right-handed double helix with one or two complete helical turns, such that the four ends of the double helix are connected in pairs in order to make a closed single-strand knot.

4.2.1 Topology of the defect loops. Knotted colloidal particles support different entanglements and spans of the topological

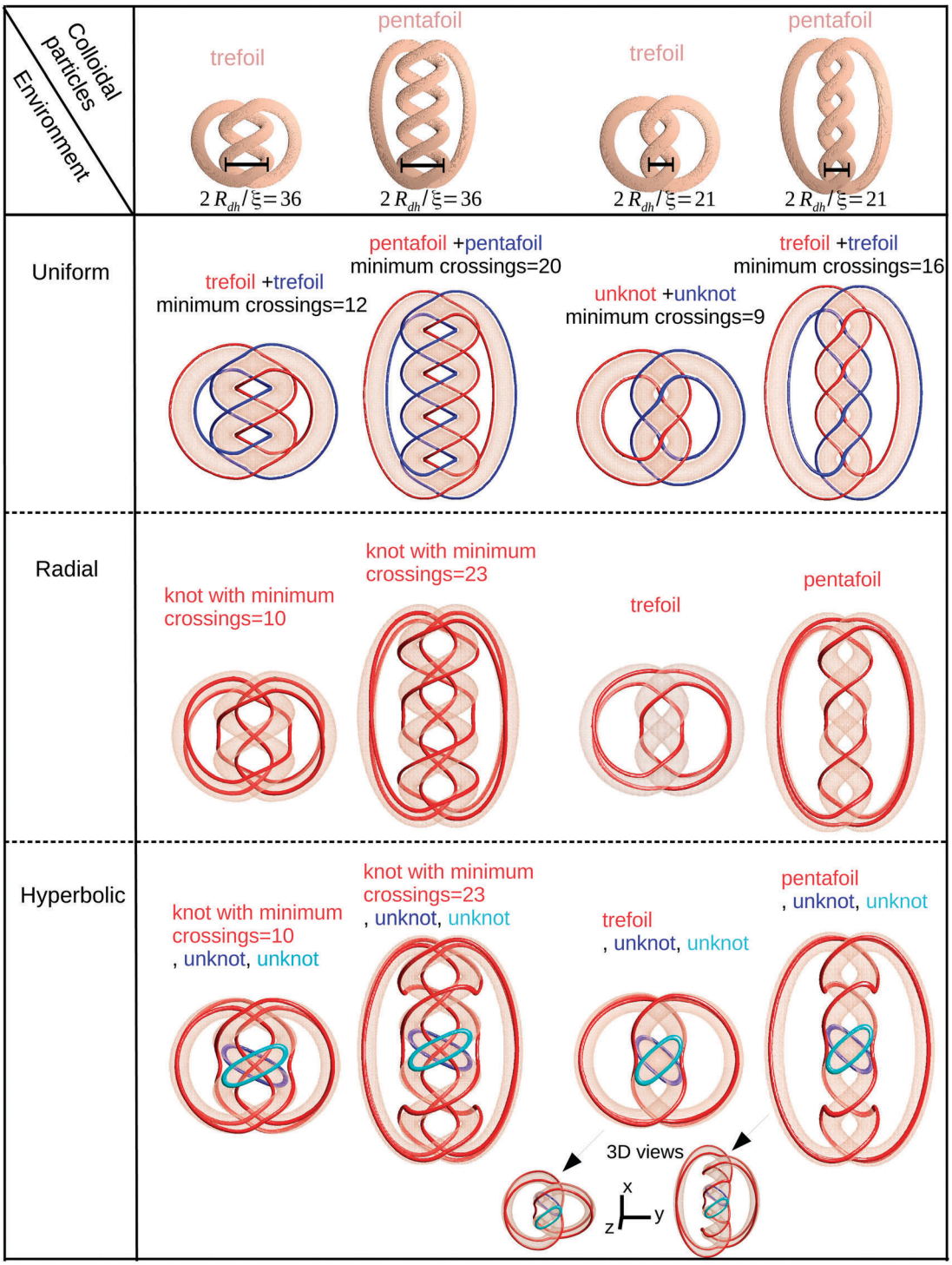

Fig. 4 Multiple knotted and linked field structures as stabilised by nematic knotted colloids in uniform, radial and hyperbolic environments. The defect structures are −1/2 disclination loops with a local along-the-loop twisted director component (more details are illustrated in Fig. 5). The stable lowest free energy configurations of the trefoil and pentafoil knotted particles with $2R_{dh}/\xi$ = 36 and $2R_{dh}/\xi$ = 21 in uniform, radial and hyperbolic environments are illustrated. The defect loops are shown by the isosurface with S = 0.3 in red, light blue and dark blue colors. The minimum crossing number associated with each of the defect loops is indicated.

defect loops depending on the position and orientation of the knotted particle. The stable configurations of the trefoil and pentafoil knotted particles in the radial, uniform and hyperbolic environments are shown in Fig. 3a–c and 4. When the center of the knotted particle is at the cavity center, the knotted particle effectively experiences the centrosymmetric pattern of the environment boundary that stabilizes the particle at the cavity center. The orientation of the knotted particle at the center of the radial

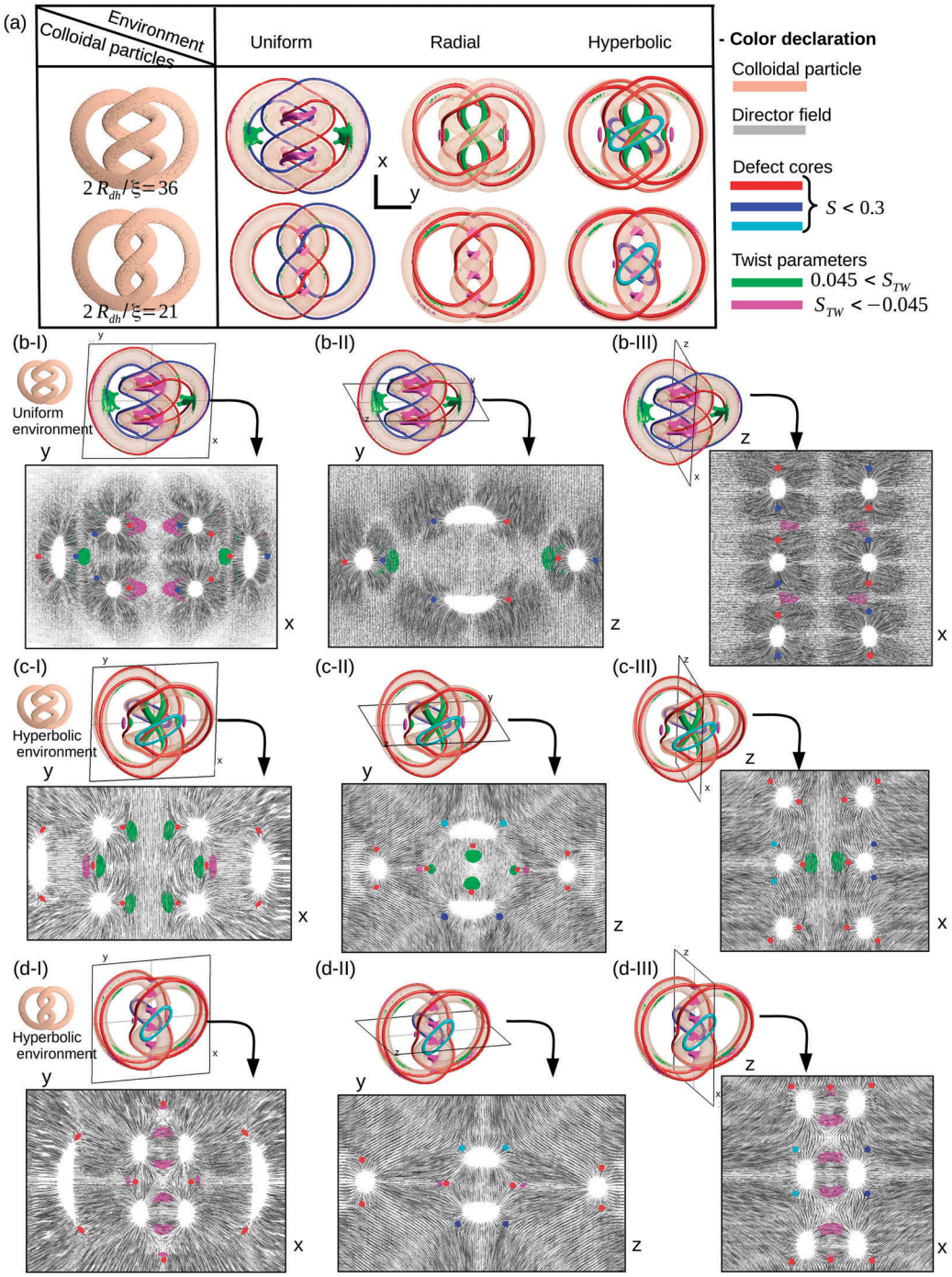

Fig. 5 Topological states of knotted nematic colloids as a combination of singular and non-singular defect structures in different topological environments. The most stable states of the trefoil knotted particles with $2R_{dh}/\xi$ = 36 and $2R_{dh}/\xi$ = 21 in radial, uniform and hyperbolic environments are illustrated. (a) The defect loops (red, light blue and dark blue colors) shown by $S < 0.3$ and the regions with large twist deformations (light green and light purple for left-handed and right-handed twists) are visualized with the twist parameter values of $0.045 < S_{TW}$ and $S_{TW} < -0.045$. (b–d) The director field (gray dashed lines) in the cross section of the cavities in *xy*, *yz* and *xz* coordinate planes. It can be seen in (b–d) that the defect loops are singular −1/2 defects with piecewise/partial along-the-loop twisted structures. The twisted-core solitonic structures are nested along the helical axis of the colloidal double helix that can be seen in the cross sections shown in b-I, c-II, d-I and d-III.

environment has continuous degeneracy because of the full rotational symmetry of the radial environment, so in this case the topological state is independent of the particle orientation. However, the topological states in the case of the uniform and hyperbolic environments are dependent of the particle orientation. Free energy values with respect to the orientation angle of the trefoil and pentafoil knot particles are presented in the graphs of Fig. 3b and c. It can be seen in the graphs of Fig. 3b and c that the minimum energy in both of the uniform and hyperbolic environments is obtained at $\theta = 0$. In what follows, we present results regarding the lowest-energy states with respect to position and orientation.

The trefoil and pentafoil knotted colloidal particles generate complex knotted or linked defect loops that are imposed by the particle shape and the environment (Fig. 4). Locally, the cross section of the defect loops shows that these are $-1/2$ disclination loops with a possible local along-the-loop twisted director component, as shown by the twist parameter S_{TW} in Fig. 5a–d. A topologically intricate defect pattern is especially imposed by the double helical segment of the particle, which can impose one or two pairs of intertwined disclination lines around the same axis of revolution as the helical axis. The number of turns of the intertwined double disclinations is related to the number of turns of the colloidal double helix. The intertwined disclinations extend out of the colloidal double helix towards the colloidal half-torus segments, where their ends are connected to the disclination half rings that form along the toroidal parts of the particle. Topologically, closed disclination knots and links form, which are further linked with the colloidal knot.

A rich variety of nematic field configurations (knots and links) can be generated by varying either the colloidal parameters, *i.e.* the double helix radius and the knot type, or the environmental patterns as shown in Fig. 4. In all the environments, the difference between the knotted and linked defect loops around the knotted particles with $2R_{dh}/\xi = 36$ and $2R_{dh}/\xi = 21$ is that in the former case there are no disclination lines, but in the latter case two intertwining disclination lines form inside the colloidal double helix. In the uniform environment, the disclination lines follow the two sides of the colloidal tube, whereas in the radial and hyperbolic environments, the disclination lines trace a different path along the colloidal tubes. One knotted defect loop forms in the radial environment and one knotted defect loop and two unlinked unknot defect loops form around the particle in the hyperbolic environment. At the level of considering defect loops as simple lines (*i.e.* without considering the surrounding director), the knotted disclination loops in the radial and hyperbolic environments are topologically-equivalent knots, which is the consequence of similar nematic patterns inside a thin volume layer at the middle of the cavity with a thickness similar to that of the knotted particle.

4.2.2 Non-singular and singular field in topological environments. Tuning the colloidal parameters that modify the distance between different parts of the colloidal surface can lead to interplay between the structuring ability of the particle and the nematic ordering imposed by the environment, allowing for different topological states to be induced in the cavity. For the distance between the coils that we considered here, the nematic configurations within the coil openings are influenced by both the particle shape and the environmental pattern, whereas the nematic configuration inside the cylindrical domain of the double helix is shielded – *i.e.* effectively screened by the surface – from the influence of the environmental pattern through the openings between the coils. However, the nematic configuration inside the double helix can be influenced by the environmental patterns through the top and bottom openings of the double helix. In the case of the double helix with a diameter of $2R_{dh}/\xi = 36$ (Fig. 5b and c), the environmental patterns through the top and bottom openings of the double helix influence the central nematic configuration, and the effect of the normal anchoring on the double helix tube remains limited near the double helix wall. In the case of the (tighter) double helix with a diameter of $2R_{dh}/\xi = 21$ (Fig. 5d), the environment-imposed pattern can not affect the nematic configuration inside the double helix, effectively making the nematic volume within the double helix unaffected by environment-imposed ordering effects. To generalise, we show that by tuning the exact parameters of the colloids (in our case the exact geometry of the double helix), one can effectively screen the role of the environment and also its topology, leading to effective compartmentalisation of the three dimensional ordering fields.

Topological environments in combination with colloidal particles of non-trivial topology also support a large variety of non-singular field states. The structures formed from the interplay between the knotted colloidal particles and the environmental patterns actually turn out to be 3D field configurations. These consist of not only knotted and linked disclination loops, but also of different types of solitonic structures residing in the field around the colloidal particle, mostly inside the area that is surrounded by the colloidal double helix (Fig. 5(b-I, c-II, d-I and d-III)). More precisely, solitonic structures are typically nonsingular defect-like regions with director configurations escaped into the third dimension within their core. In the case of the double helix with a diameter of $2R_{dh}/\xi = 36$, local escaped defects form along the symmetry axis of the colloidal double helix (Fig. 5(b-I and c-II)) which are affected by the environmental patterns. In the case of the double helix with a diameter of $2R_{dh}/\xi = 21$, the environmental patterns do not penetrate inside the colloidal double helix, so the escaped defects along the helical axis of the colloidal double helix (Fig. 5(d-I and d-III)) are only related to the specific shape of the double helix. In this case, the nematic topological state within the area inside the double helix is a chiral nematic configuration with the same helical pitch and handedness as the colloidal double helix. In this case, no disclinations form along the internal walls of the double helix, and the lack of disclination is compensated by the formation of solitonic topological structures that are usually observed in chiral nematic media, but here are imprinted by the colloidal double helix in achiral nematic media. Considering the literature, we refer to these solitonic structures as baby merons (Fig. 6), in which director rotations of 180° or less are observed along the lines that pass across the solitonic structure core, in comparison with a complete meron structure that is characterized by a 180° twisted

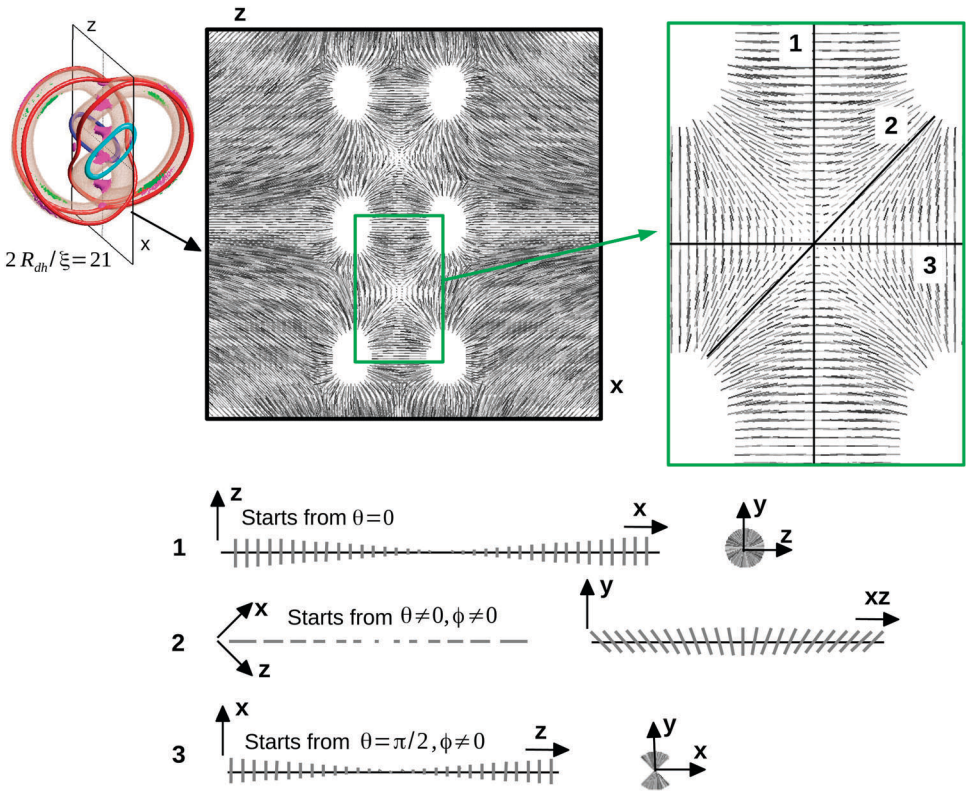

Fig. 6 Twisted core solitonic structures called baby merons. The director field in a cross section of the colloidal double helix with a diameter of $2R_{dh}/\xi$ = 21 in a hyperbolic environment is illustrated as a typical example of baby merons, which are also observed in the case of the radial and uniform environments inside the colloidal double helix with a diameter of $2R_{dh}/\xi$ = 21. The rotation direction of the director field along three different lines across the core of a baby meron is illustrated from two different views that show a 180° twist or less in the director orientations.

director field along all the lines crossing its core.[34] We have observed the same baby meron structures in radial, uniform and hyperbolic environments, and in all the cross section planes containing the symmetry axis of the double helix, which only differ by the positioning of their cores along the helical axis in these planes.

5 Conclusions

In this paper, we considered three different designs for the topological structures of the environment in a system of trefoil and pentafoil nematic colloidal knots. Achiral nematic cavities with three structured surface patterns are shown to create smoothly-varying environmental profiles: radial, uniform, and hyperbolic. From the view of the nematic elastic free energy, these environments are characterized by no deformation of the nematic in the uniform environment, pure 3D splay deformation in the radial environment, and a combination of splay and bend deformations in the hyperbolic environment. The considered environmental patterns impose no chirality; however, several chiral nematic structures are stabilised as a result of particle shape and orientation, with respect to the environmental patterns.

To generalise, colloidal particles in nematics can stabilise nematic topological states based on their geometric and topological characteristics, as further complemented by the complexity of the nematic environment itself, which can impose and energetically stabilise further topological structures. For example, in a chiral nematic medium with a radial surface anchoring pattern, even in the absence of colloidal particles, an abundance of diverse defect points and loops and solitonic structures can be stabilized all over the droplet.[24,25,32] But, in the case of smoothly-varying environmental nematic patterns in an achiral nematic medium, similar to what we have studied here, topological defects and other topological structures can be stabilised by colloidal particles, and are a direct realization of the interplay between particle-imposed and environment-imposed nematic ordering. In this case, the topological states adapt to the geometric shape of the colloidal particles, such as knotted and linked defect loops that are imposed by knotted and linked colloidal particles, but with the structure also crucially affected by the environment.

Specifically, as less is known about how a non-trivial topology of the environment couples to the material states of topologically non-trivial particles, in this paper we focus on showing the significant influence of the topology of the environment on complex nematic states. We show that different environmental patterns can induce different structures, locations and the number of topological defects in nematic media. We show that structures of different topology – including different types of knotted and

linked fields and solitonic structures – can be generated also by tuning only selected geometric parameters of the colloidal particles, such as the openings between the double helix coils or its top and bottom openings as in our study, for example. We observe a variety of knotted nematic fields in different environments that are different adaptations of the knotted shape of the colloidal particles. We also observe several escaped-core defect-like solitonic structures, such as meron structures, that have been observed in previous studies in chiral nematic media, but are here imprinted in achiral nematic media as a result of the chiral shape of the double helix segment that is also affected by different environmental patterns. The difference between these topological states originates from interplay between the ordering imposed by the particle surfaces and the ordering imposed by the environment as given by the screening of the nematic distortion. Specifically, we show that in the case of a tight enough colloidal double helix, when the effect of the environmental patterns are completely screened by the colloidal surface, chiral nematic configurations are imposed within the area inside the double helix with the same helical pitch and handedness as the double helix. More generally, this work aims at contributing to the understanding of the role of the topology of the environment as one of the fundamental controlling mechanisms in the design of novel field and defect structures in complex soft matter.

Conflicts of interest

There are no conflicts to declare.

Acknowledgements

S. M. H. would like to thank Simon Čopar for valuable discussions on the topological charge of the environments and knot identification. The authors acknowledge financial support from the Slovenian Research Agency Grants J1-7300, L1-8135, and P1-0099.

References

1 G. V. Lauder, *J. Theor. Biol.*, 1982, **97**, 57–67.
2 L. D. Gelb, K. E. Gubbins, R. Radhakrishnan and M. Sliwinska-Bartkowiak, *Rep. Prog. Phys.*, 1999, **62**, 1573.
3 B. Yu, P. Sun, T. Chen, Q. Jin, D. Ding, B. Li and A. Shi, *Phys. Rev. Lett.*, 2006, **96**, 138306.
4 X. L. Qi and S. C. Zhang, *Phys. Today*, 2010, **63**, 33–38.
5 C. L. Kane and T. C. Lubensky, *Nat. Phys.*, 2014, **10**, 39–45.
6 X.-L. Qi, T. L. Hughes, S. Raghu and S.-C. Zhang, *Phys. Rev. Lett.*, 2009, **102**, 187001.
7 J.-H. Kim, M. Yoneya and H. Yokoyama, *Nature*, 2002, **420**, 159.
8 X. Wang, D. S. Miller, J. J. de Pablo and N. L. Abbott, *Adv. Funct. Mater.*, 2014, **24**, 6219–6226.
9 U. Tkalec, M. Ravnik, S. Čopar, S. Žumer and I. Muševič, *Science*, 2011, **333**, 62–65.
10 A. Martinez, M. Ravnik, B. Lucero, R. Visvanathan, S. Žumer and I. I. Smalyukh, *Nat. Mater.*, 2014, **13**, 258–263.
11 P. G. de Gennes, *Simple Views On Condensed Matter*, World Scientific, 2003, pp. 215–217.
12 X. R. Bao, H. J. Lee and S. R. Quake, *Phys. Rev. Lett.*, 2003, **91**, 265506.
13 F. B. Dean, A. Stasiak, T. Koller and N. R. Cozzarelli, *J. Biol. Chem.*, 1985, **260**, 4975–4983.
14 H. Wang, R. J. Di Gate and N. C. Seeman, *Proc. Natl. Acad. Sci. U. S. A.*, 1996, **93**, 9477–9482.
15 E. Orlandini and S. G. Whittington, *Rev. Mod. Phys.*, 2007, **79**, 611.
16 J. F. Ayme, J. E. Beves, C. J. Campbell and D. A. Leigh, *Chem. Soc. Rev.*, 2013, **42**, 1700–1712.
17 M. R. Dennis, R. P. King, B. Jack, K. OHolleran and M. J. Padgett, *Nat. Phys.*, 2010, **6**, 118–121.
18 D. Kleckner, L. H. Kauffman and W. T. M. Irvine, *Nat. Phys.*, 2016, **12**, 650–655.
19 E. Babaev, *Phys. Rev. B: Condens. Matter Mater. Phys.*, 2009, **79**, 104506.
20 H. K. Moffatt, *J. Fluid Mech.*, 1969, **35**, 117–129.
21 I. I. Smalyukh, Y. Lansac, N. A. Clark and R. P. Trivedi, *Nat. Mater.*, 2010, **9**, 139–145.
22 T. Machon and G. P. Alexander, *Proc. Natl. Acad. Sci. U. S. A.*, 2013, **110**, 14174–14179.
23 M. Tasinkevych, M. G. Campbell and I. I. Smalyukh, *Proc. Natl. Acad. Sci. U. S. A.*, 2014, **111**, 16268–16273.
24 D. Seč, S. Čopar and S. Žumer, *Nat. Commun.*, 2014, **5**, 3057.
25 T. Orlova, S. J. Aßhoff, T. Yamaguchi, N. Katsonis and E. Brasselet, *Nat. Commun.*, 2015, **6**, 7603.
26 D. Rolfsen, *Knots and links*, American Mathematical Soc., 1976, vol. 346.
27 J. Hoste, M. Thistlethwaite and J. Weeks, *Math. Intel.*, 1998, **20**, 33–48.
28 J.-i. Fukuda and S. Žumer, *Nat. Commun.*, 2011, **2**, 246.
29 B. G.-g. Chen, P. J. Ackerman, G. P. Alexander, R. D. Kamien and I. I. Smalyukh, *Phys. Rev. Lett.*, 2013, **110**, 237801.
30 M. Pandey, T. Porenta, J. Brewer, A. Burkart, S. Čopar, S. Žumer and I. I. Smalyukh, *Phys. Rev. E: Stat., Nonlinear, Soft Matter Phys.*, 2014, **89**, 060502.
31 Y. Guo, S. Afghah, J. Xiang, O. D. Lavrentovich, R. L. B. Selinger and Q.-H. Wei, *Soft Matter*, 2016, **12**, 6312–6320.
32 G. Posnjak, S. Čopar and I. Muševič, *Sci. Rep.*, 2016, **6**, 26361.
33 L. Cattaneo, Ž. Kos, M. Savoini, P. Kouwer, A. Rowan, M. Ravnik, I. Muševič and T. Rasing, *Soft Matter*, 2016, **12**, 853–858.
34 T. Machon and G. P. Alexander, *Proc. R. Soc. A*, 2016, **472**, 20160265.
35 P. J. Ackerman and I. I. Smalyukh, *Phys. Rev. X*, 2017, **7**, 011006.
36 N. D. Mermin, *Rev. Mod. Phys.*, 1979, **51**, 591.
37 A. Saupe, *Mol. Cryst. Liq. Cryst.*, 1973, **21**, 211–238.
38 M. V. Kurik and O. D. Lavrentovich, *Phys.-Usp.*, 1988, **31**, 196–224.
39 A. Martinez, L. Hermosillo, M. Tasinkevych and I. I. Smalyukh, *Proc. Natl. Acad. Sci. U. S. A.*, 2015, **112**, 4546–4551.
40 H. Löwen, *J. Phys.: Condens. Matter*, 2001, **13**, R415.
41 Y. Min, M. Akbulut, K. Kristiansen, Y. Golan and J. Israelachvili, *Nat. Mater.*, 2008, **7**, 527–538.

42 L. Tran, M. O. Lavrentovich, G. Durey, A. Darmon, M. F. Haase, N. Li, D. Lee, K. J. Stebe, R. D. Kamien and T. Lopez-Leon, *Phys. Rev. X*, 2017, **7**, 041029.
43 X. Wang, Y. Zhou, Y. K. Kim, D. S. Miller, R. Zhang, J. A. Martinez-Gonzalez, E. Bukusoglu, B. Zhang, T. M. Brown, J. J. de Pablo and N. L. Abbott, *Soft Matter*, 2017, **13**, 5714–5723.
44 E. Pairam, J. Vallamkondu, V. Koning, B. C. van Zuiden, P. W. Ellis, M. A. Bates, V. Vitelli and A. Fernandez-Nieves, *Proc. Natl. Acad. Sci. U. S. A.*, 2013, **110**, 9295–9300.
45 V. Y. Zyryanov, M. N. Krakhalev, O. O. Prishchepa and A. V. Shabanov, *JETP Lett.*, 2008, **88**, 597–601.
46 M. G. Campbell, M. Tasinkevych and I. I. Smalyukh, *Phys. Rev. Lett.*, 2014, **112**, 197801.
47 S. Candau, P. Le Roy and F. Debeauvais, *Mol. Cryst. Liq. Cryst.*, 1973, **23**, 283–297.
48 G. E. Volovik and O. D. Lavrentovich, *Zh. Eksp. Teor. Fiz.*, 1983, **85**, 1997–2010.
49 P. G. de Gennes and J. Prost, *The physics of liquid crystal*, Oxford University Press, 1995.
50 M. Ravnik and S. Žumer, *Liq. Cryst.*, 2009, **36**, 1201–1214.
51 C. Geuzaine and J.-F. Remacle, *Int. J. Numer. Meth. Eng.*, 2009, **79**, 1309–1331.
52 S. Čopar, T. Porenta, V. S. R. Jampani, I. Muševič and S. Žumer, *Soft Matter*, 2012, **8**, 8595–8600.
53 C. Peng, Y. Guo, T. Turiv, M. Jiang, Q.-H. Wei and O. D. Lavrentovich, *Adv. Mater.*, 2017, **29**, 1–6.
54 J. Genzer and R. R. Bhat, *Langmuir*, 2008, **24**, 2294–2317.
55 M. M. Norton, A. Baskaran, A. Opathalage, B. Langeslay, S. Fraden, A. Baskaran and M. F. Hagan, *Phys. Rev. E*, 2018, **97**, 012702.
56 I. C. Gârlea, P. Mulder, J. Alvarado, O. Dammone, D. G. Aarts, M. P. Lettinga, G. H. Koenderink and B. M. Mulder, *Nat. Commun.*, 2016, **7**, 12112.
57 M. Škarabot, M. Ravnik, S. Žumer, U. Tkalec, I. Poberaj, D. Babič and I. Muševič, *Phys. Rev. E: Stat., Nonlinear, Soft Matter Phys.*, 2008, **77**, 061706.